Geometrical model of spiking and bursting neuron on a mug-shaped branched manifold

Mohamed Gheouali, Tounsia Benzekri, René Lozi, Guanrong Chen

To be published in

International Journal of bifurcation and Chaos
December, 2020

Geometrical model of spiking and bursting neuron on a mug-shaped branched manifold

Mohamed Gheouali
University of Sciences and Technologies Houari Boumediene (USTHB), Mathematical Faculty, 16111 El Alia, Bab Ezzouar, Algeria.
mohamegheouali@gmail.com

Tounsia Benzekri
University of Sciences and Technologies Houari Boumediene (USTHB), Mathematical Faculty, 16111 El Alia, Bab Ezzouar, Algeria.
tbenzekri@usthb.dz

René Lozi
University of Nice Sophia-Antipolis, U.C.A., UMR CNRS 7351, Nice, France
Rene.LOZI@univ-cotedazur.fr *

Guanrong Chen
Department of Electrical Engineering, City University of Hong Kong, Hong Kong SAR, China
gchen@ee.cityu.edu.h

Received (to be inserted by publisher)

Based on the Hodgkin-Huxley and Hindmarsh-Rose models, this paper proposes a geometric phenomenological model of bursting neuron in its simplest form, describing the dynamic motion on a mug-shaped branched manifold, which is a cylinder tied to a ribbon. Rigorous mathematical analysis is performed on the nature of the bursting neuron solutions: the number of spikes in a burst, the periodicity or chaoticity of the bursts, etc. The model is then generalized to obtain mixing burst of any number of spikes. Finally, an example is presented to verify the theoretical results.

Keywords: Bursting oscillation; Spike, Poincaré map, Horseshoe attractor, Chaos.

1. Introduction

In the human brain, which is believed to be the most complex of all biological systems, there are more that 100 billion of biological neurons. Each neuron is connected to many others (up to 10,000) via synapses in intricate patterns [Stiles & Jernigan, 2010]. Neuronal signals consist of short electrical pulses, which can be observed by placing a fine electrode close to the soma or axon of a neuron. These neurons may present *spiking* and *bursting* activities. Since all *spikes* of a given neuron look alike, the form of the action potential does not carry much information. Rather, it is the number and the timing of *spikes* that matter. However, because *spiking-bursting* activities result from higher-dimensional nonlinear dynamics of various

*rlozi@unice.fr

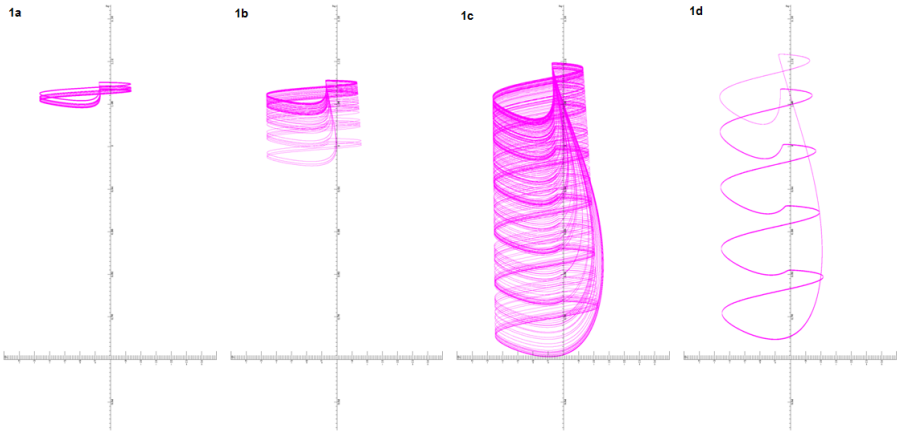

Figure 1. Solution of the Hindmarsh-Rose equation on the (y, z) plane for $a = 1, b = 3, c = -3, d = 5, s = 4, I = 5, x_1 = -1.03$. Initial values $x_0 = 0, y_0 = 2.22, z_0 = 1$ and different values of ϵ: $1a$, $\epsilon = 0.0013$, $1b$, $\epsilon = 0.0165$, $1c$, $\epsilon = 0.04$, $1d$, $\epsilon = 0.05$.

ionic currents flowing through the membrane channels, it is very difficult to model exactly all the biochemical reactions that are interacting in a single neuron.

Since the pioneering works of Hodgkin and Huxley [Hodgkin & Huxley, 1952] (the H-H model), which studied the squid giant axon, several channel-based models composing of several nonlinear equations have been designed to capture the physiological processes in the membrane (see [Shilnikov & Rulkov, 2003; Shilnikov & Kolomiets, 2008] for a survey). Contrarily, phenomenological models try only to replicate the characteristic features of the *bursting* behavior without direct relating to what happens in the neuron from a biological perspective. Among them, the most known is the Hindmarsh-Rose model [Corson, 2009] (the H-R model). In their first paper dated 1982, Hindmarsh and Rose introduced a model of two ordinary differential equations (ODE), which comes from a modification of the Fitzhugh-Nagumo system derived from a two-equation reduction of the H-H model of four ODE [Hindmarsh & Rose, 1982]. Two years later in [Hindmarsh & Rose, 1984], they expanded their simple 2-D into a more sophisticated 3-D model, which demonstrates almost all types of robust activities in the H-H model:

$$\begin{cases} \dot{x}(t) = y(t) - ax^3(t) + bx^2(t) + I - z(t), \\ \dot{y}(t) = c - dx^2(t) - y(t), \\ \dot{z}(t) = \epsilon(s(x(t) - x_1) - z(t)). \end{cases} \tag{1}$$

In this model, the voltage across the neuron's membrane is represented by the variable x, meanwhile the other two variables y and z describe some ionic currents' kinetics. Because the parameter ϵ is small, system (1) is called a slow-fast system. Both H-H and H-R models have been thoroughly and extensively studied using dynamic systems theory and tools. However, due to the innermost nonlinearities, system (1) is not easy for strictly mathematical proofs of solution properties. Moreover, small change in one of the seven parameters, a, b, c, d, I, ϵ, x_1, can lead to very different solutions (see Fig. 1).

Aside from the H-R model, the FitzHugh-Nagumo (FHN) system, modeled by a two-dimensional nonlinear differential equation, when used with fractional derivative (Fractional FitzHugh-Nagumo FFHN), exhibits Mixed-Mode Oscillations (MMO) similar to the *burst* of *spikes* of the H-H model [Abdelouahab *et al.*, 2019].

In what follows, we introduce a geometric phenomenological model of *bursting* neuron, which has some similarities with the H-R model. This model, which defines motion on a mug-shaped branched manifold, is presented in its simplest form where the branched manifold is simply a cylinder tied to a ribbon. This model belongs to a family of geometrical models for which the cylinder can be replaced by a cone or a paraboloid and the single ribbon can be duplicated. This geometrical mug-shaped model allows some rigorous mathematical analysis on the nature of its solutions: the number of *spikes* in a *burst*, the periodicity or chaoticity of the *bursts*, etc.

Next, in Sec. 2, the simplest geometric mug-shaped model on a branched manifold is defined. This

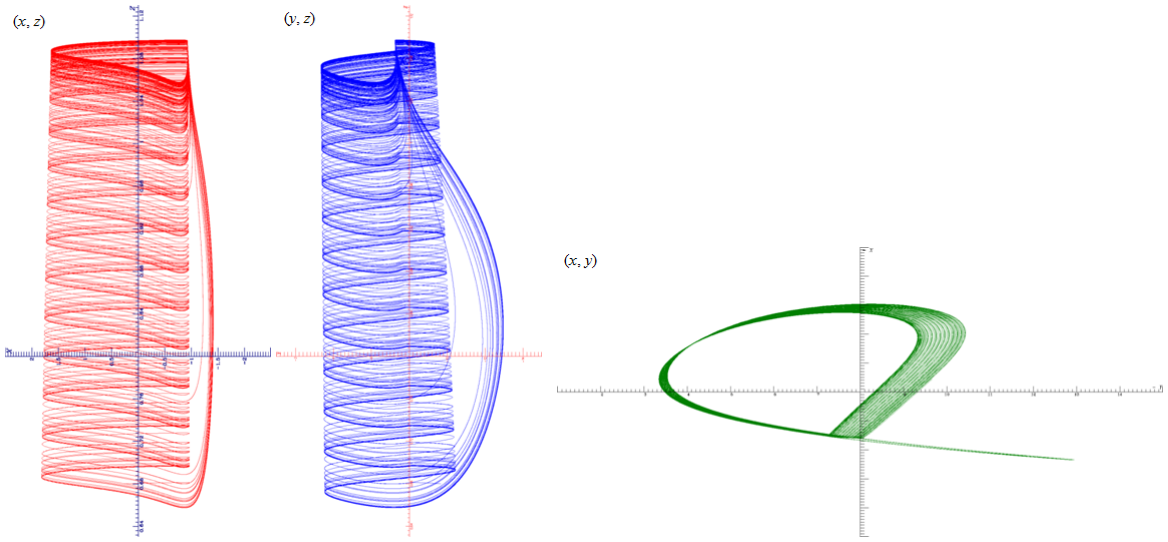

Figure 2. Solution of the Hindmarsh-Rose equation on the $(x, z), (y, z), (x, y)$ planes for $a = 1, b = 3, c = -3, d = 5, s = 4, I = 5, x_1 = -1.03, \epsilon = 0.002$. Initial values $x_0 = 0, y_0 = 2.22, z_0 = 1$.

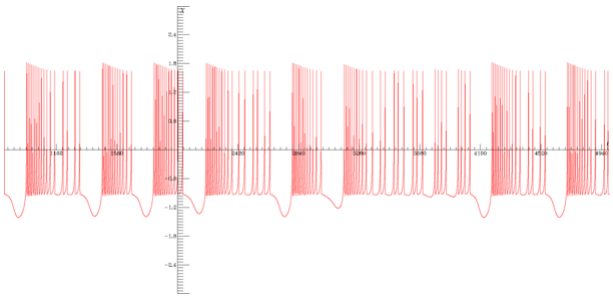

Figure 3. Solution of the Hindmarsh-Rose equation on the (x, t), coordinates for $a = 1, b = 3, c = -3, d = 5, s = 4, I = 5, x_1 = -1.03, \epsilon = 0.002$. Initial values $x_0 = 0, y_0 = 2.22, z_0 = 1$.

simplest model generates only *bursting* orbits, which mix *burst* of n and $n + 1$ *spikes*. In Sec. 3, properties of periodic and quasiperiodic orbits are studied, and rigorous proofs of their existence are given. In Sec. 4, a more complex case of the model is studied, which generates chaotic *bursting* orbits with *burst* of n and $n+1$ *spikes*. In Sec. 5, the model is generalized to obtain mixing *burst* of any number of *spikes*. An example with *bursts* of 4 to 8 *spikes* is discussed. Finally, in Sec. 6, a brief conclusion is drawn.

2. Geometrical model of neuron on a mug-shaped branched manifold: simplest case

In this section, a new model of neuron defined on manifold is introduced, inspired the shape of solutions of the H-R model. Fig. 2 shows a solution of the Hindmarsh-Rose equation on the (x, z), (y, z), and (x, y) planes. Figure 3 displays the x signal versus time, highlighting the *spiking-bursting* phenomenon.

Then, a mug-shaped branched manifold is introduced, consisting of a cylinder of finite length connected to a ribbon defined using a sheaf of rectangular part on the plane (Fig. 4). The geometrical model is defined by curves circling upward around this cylinder, and jumping back to its basis through the ribbon, when they cross a threshold on the upper part of the cylinder (Fig. 5).

Formally, the dynamics on the mug-shaped manifold is composed of two folds: the dynamics on the cylinder, and the dynamics on the ribbon.

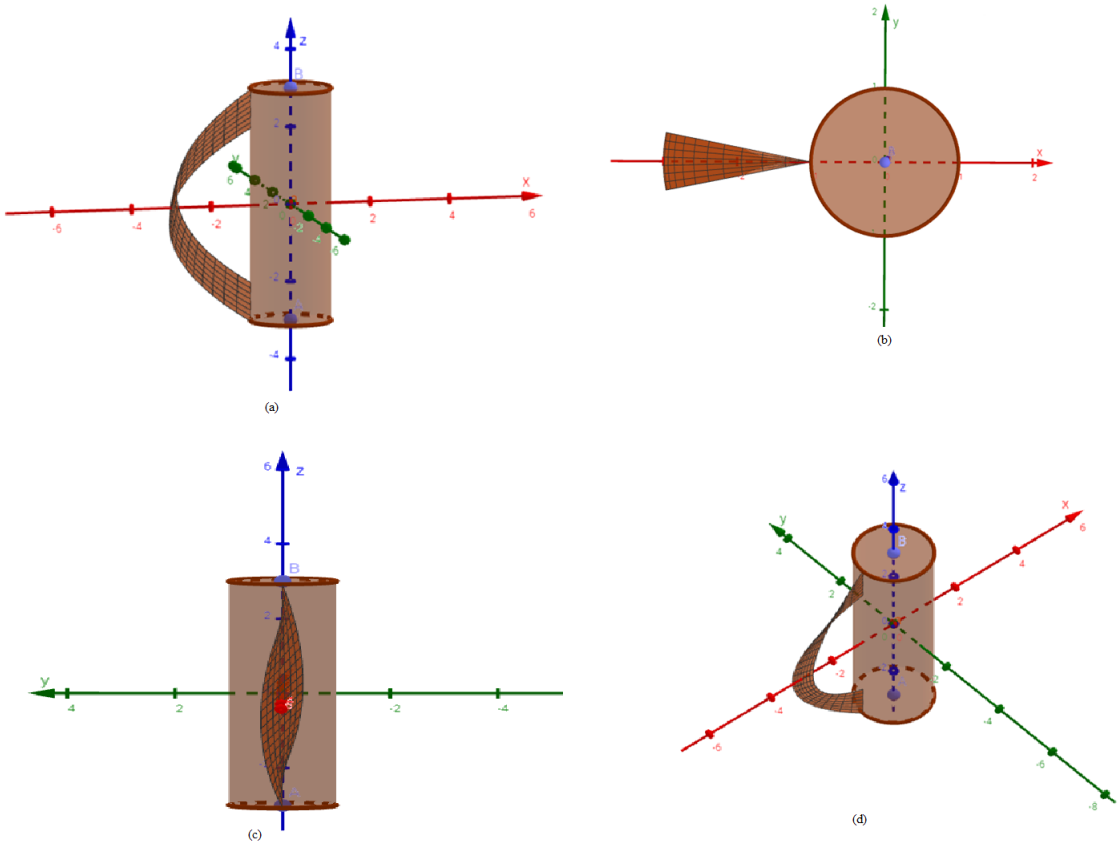

Figure 4. Ribbon and cylinder view in perspective in coordinate (O, x, y, z) . (a) side view, (b) projection on the plane (x, y), (c) projection on the plane (y, z), (d) top view

2.1. *Dynamics on the cylinder*

Let S of $\mathbb{R}^3$ be the cylindrical region defined by $x^2 + y^2 = 1$ and $-s - 1 \leqslant z \leq s + 1$, where $s \in \mathbb{R}^+$ is the half length of the cylinder.

We first define precisely what we call *spike*, *burst* and *bursting* trajectories (or *bursting* orbit, or *bursting* solution) of the geometrical model.

2.1.1. *Spike, burst and bursting orbits*

As shown in Fig. 3, a *spike* in the H-R model (1) is the projection of a complete revolution of the signal around the z axis, on the (x, t) coordinates. In the same manner, a *spike* in the geometrical model corresponds to the part of the trajectory turning around the cylinder.

A *burst* occurs when neuron activity alternates between a quiescent state and repetitive *spiking* as shown in Fig. 6 [Izhikevich, 2007]. In the proposed geometrical model, a *burst* is a piece of the trajectory starting from the lower part of the cylinder, circling many times around it, leaving the cylinder as soon as it can escape from it to the top part of the ribbon, and ending at the boundary between the low part of the ribbon and the cylinder.

A *bursting* orbit $\mathcal{B}(z_0)$ is a continuous trajectory encompassing an infinite sequence of *bursts* $\mathcal{B}(z_0) = \{B_0(z_0), B_1(z_0), ..., B_m(z_0), ...\}$ defined by its initial point $(-1, 0, z_0)$ at the initial time t_0, $z_0 = z(t_0)$.

It can be periodic, pseudo-periodic or chaotic.

Now, assume that for the *burst* $B_{m_{(z_0)}}$, the trajectory starts to turn around the cylinder at the time $\tau^c_{m_{(z_0)}}$ and the point $(-1, 0, z(\tau^c_{m_{(z_0)}}))$, with $-s - 1 \leq z(\tau^c_{m_{(z_0)}}) < -s$, and leaves the cylinder S at the time

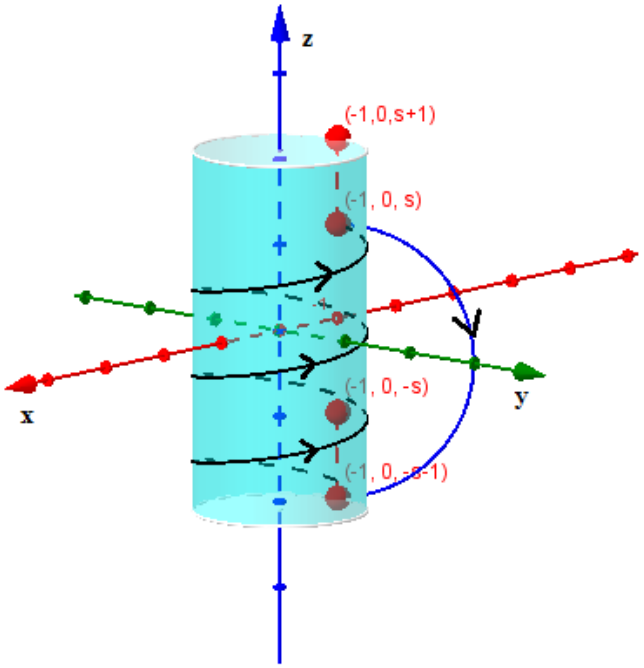

Figure 5. Geometrical representation of dynamics of a neuron on the cylinder S

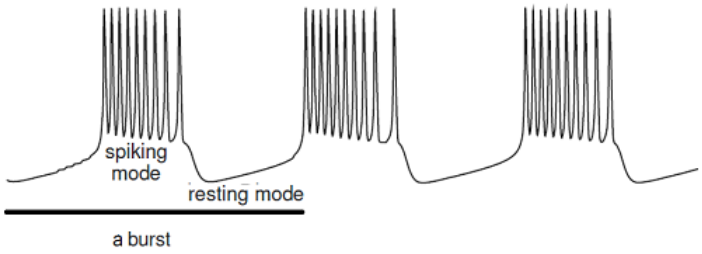

Figure 6. *Bursting* trajectory with three *bursts* [Izhikevich, 2007].

$\tau^r_{m_{(z_0)}}$ and the point $(1, 0, z(\tau^r_{m_{(z_0)}}))$, with $s \leq z(\tau^r_{m_{(z_0)}}) < s + 1$, to traverse on the ribbon.

The point $(-1, 0, z(\tau^c_{m_{(z_0)}}))$ for $m > 1$ is defined as the end of the trajectory of $B_{m-1_{(z_0)}}$, which in turn is defined by $B_{m-2_{(z_0)}}$ and recursively by $B_{m-3_{(z_0)}}, ..., B_{2_{(z_0)}}, B_{1_{(z_0)}}$ and by $\tau^c_{0_{(z_0)}} = t_0$ for $B_{0_{(z_0)}}$.
For simplicity, in the case where no ambiguity can occur, denote $\tau^r_{m_{(z_0)}}$ (resp. $\tau^c_{m_{(z_0)}}$) by τ^r_m, (resp. τ^c_m) and $B_{m_{(z_0)}}$ by B_m.

The duration of this *burst* is equal to $\tau^c_{m+1} - \tau^c_m$ i.e.

$$t \in T^B_m = [\tau^c_m, \tau^c_{m+1}[= T^{Bcyl}_m \cup T^{Brib}_m = [\tau^c_m, \tau^r_m[\cup [\tau^r_m, \tau^c_{m+1}[.$$

The number of *spikes* within a *burst* is the total number of turns that the *bursting* orbit did around the cylinder S.

2.1.2. *Intervals of injection and reinjection*

Here, consider a trajectory which arrives from the ribbon and begins to turn around the cylinder.

Definition 2.1. Interval of reinjection
Let $I_s^c = [-s-1, -s[$ be an interval of the z-axis, and $\bar{I}_s^c = \{-1\} \times \{0\} \times I_s^c$ be the interval that contains all possible initial points of trajectories of the geometrical model, leaving the ribbon to turn around the cylinder. This interval is called the interval of reinjection.

Definition 2.2. Interval of injection
Let $I_s^r = [s, s+1[$ be an interval of the z-axis, and $\bar{I}_s^r = \{-1\} \times \{0\} \times I_s^r$ be the interval that contains all possible final points of trajectories of the geometrical model, leaving the cylinder to move to the ribbon. This interval is called the interval of injection.

For simplicity, in the rest of this article, we identify the point $(-1, 0, z) \in \{-1\} \times \{0\} \times [-s-1, -s[$ as the point $z \in [-s-1, -s[$ of the z-axis and the point $(-1, 0, z) \in \{-1\} \times \{0\} \times [s, s+1[$ as the point $z \in [s, s+1[$ of the z-axis, see Fig. 5. Consequently, we identify the interval $\bar{I}_s^c$ (resp. $\bar{I}_s^r$) with the interval I_s^c (resp. I_s^r).

2.1.3. *Equation of trajectories on the cylinder*

In order to define, in a simplified manner, the equations of the motion belonging to the cylinder, in every *burst* B_m, use the local time θ:

$$\forall\ t \in T_m^{Bcyl},\ \theta = t - \tau_m^c. \tag{2}$$

For $\theta \in [0, \tau_m^r - \tau_m^c[$, equations of motion are given by the following differential equations:

$$\begin{cases} \ddot{x}(\theta) = -4\pi^2 x(\theta), \\ \ddot{y}(\theta) = -4\pi^2 y(\theta), \\ \dot{z}(\theta) = 1. \end{cases} \tag{3}$$

Then, in the case where the *spikes* are regularly spaced, at each *burst* B_m the solution on the cylinder is given by

$$\begin{cases} x(\theta) = \cos(2\pi\theta + \pi), \\ y(\theta) = \sin(2\pi\theta + \pi), \\ z(\theta) = \theta + z_m^c. \end{cases} \tag{4}$$

The initial condition of the solution in B_m verifies $z_m^c \in I_s^c$. During the *burst*, this solution is turning around the cylinder, as long as $z(\theta) < s$, until $x(\theta) \neq -1$.

When $z(\theta) \geqslant s$ and $x(\theta) = -1$, the trajectory leaves the cylinder and traverses on the ribbon.

2.1.4. *The half-Poincaré map on the cylinder*

In this article, consider only the case where *spikes* are regularly spaced versus time at the same *burst*. This is due to the third equation of (3), $\dot{z}(\theta) = 1$. However, it is easy to relax this constraint, allowing more flexibility to the behavior of the *spike*, by modifying slightly this equation as $\dot{z}(\theta) = f(\theta)$, with for example $f(\theta) = \theta + \frac{1}{2}$.

At any *burst*, the trajectory starting from interval $\bar{I}_s^c$ must eventually exit from S through $\bar{I}_s^r$. Since the interval $\bar{I}_s^c$ (resp. $\bar{I}_s^r$) is identified with the interval I_s^c (resp. I_s^r), one can define a map $\Psi_1 : I_s^c \longrightarrow I_s^r$

following trajectories that start from I_s^c until they first meet I_s^r: $\Psi_1(z_m^c) = z(\tau_m^r) = z_m^r$. For all $z_m^c \in I_s^c$, there is $\theta^* = k, k \in \mathbb{N}$, such that $\Psi_1(z_m^c) = k + z_m^c$, for which one has

$$s \leq k + z_m^c < s + 1,$$

because $x(\theta^*) = -1$ and $y(\theta^*) = 0$. By writing $2s$ as $2s = [2s] + \alpha, 0 \leq \alpha < 1$, one has

$$[2s] + (-z_m^c - s + \alpha) \leq k < [2s] + (-z_m^c - s + \alpha) + 1.$$

From the fact that

$$\begin{cases} 1 \leq (-z_m^c - s + \alpha) < 2 & \text{for} \quad z_m^c \in [-s-1, -s-1+\alpha[, \\ 0 < (-z_m^c - s + \alpha) \leq 1 & \text{for} \quad z_m^c \in [-s-1+\alpha, -s[, \end{cases}$$

it follows that

$$k = \begin{cases} [2s] + 2 & \text{for} \quad z_m^c \in [-s-1, -s-1+\alpha[, \\ [2s] + 1 & \text{for} \quad z_m^c \in [-s-1+\alpha, -s[. \end{cases}$$

Therefore, one has $\Psi_1 : I_s^c \longrightarrow I_s^r$ defined by

$$\Psi_1(z) = \begin{cases} z + [2s] + 2 & \text{for} \quad z \in [-s-1, -s-1+\alpha[, \\ z + [2s] + 1 & \text{for} \quad z \in [-s-1+\alpha, -s[. \end{cases} \tag{5}$$

(See example with $s = 2.2$, shown in Fig. 7).

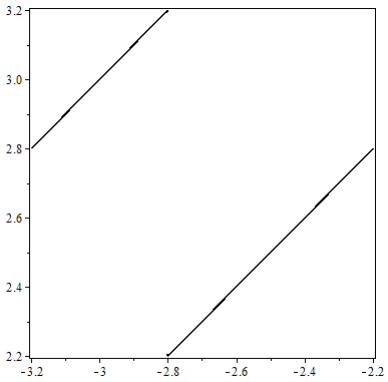

Figure 7. The graph of the map Ψ_1 for $s = 2.2$

At a *burst*, as will be seen in Section 3, this map can define patterns of $[2s] + 1$ and $[2s] + 2$ *spikes*.

This half-Poincaré map is coupled with a second half-Poincaré map on the ribbon linking the interval of injection to the interval of reinjection.

2.2. *Dynamics on the ribbon*

When $x = -1$ and $z \geq s$, the orbits leave the cylinder S towards the plane (x, z) to form the phase of quiescence and then return to the cylinder.

Here, assume that the duration between *bursts* (*interbursts* or *interspikes*), representing the phase of quiescence, is the same for all *bursts* and is equal to $2T$.

$$T_m^{Brib} = [\tau_m^r, \tau_{m+1}^c[= [\tau_m^r, \tau_m^r + 2T[. \tag{6}$$

2.2.1. *Ribbon defined by a sheaf of rectangular part of plane*

On the ribbon, just like on the cylinder, define in every *burst* B_m the local time

$$\theta : \forall\ t \in T_m^{Brib},\ \theta = t - \tau_m^r \in [0, 2T[. \tag{7}$$

Also, assume that the projection on the z-axis of every trajectory on the ribbon has the same length $2s+1$, and has a parabolic shape. Due to the Poincaré-Bendixon theorem, which implies that on a plane no trajectory of a dynamical system can cross another trajectory, the ribbon cannot belong to a single plane. In order to avoid such inappropriate crossing, define each identical parabola-shaped trajectory on a separate half-plane H_m, formed by the angle $\hat{\mu}_m$ between H_m and the half-plane $H = \left\{X \geq 0, (Y, Z) \in \mathbb{R}^2\right\}$, for which both systems of coordinates (O, x, y, z) and $\left(\tilde{O}, X, Y, Z\right)$ are defined by

$$\begin{cases} X = x + 1, \\ Y = y, \\ Z = z, \end{cases} \tag{8}$$

and $\tilde{O} = (-1, 0, 0)$ in the system (O, x, y, z), together with the family of systems of coordinates $\left(\tilde{O}, \tilde{X}_m, \tilde{Y}_m, \tilde{Z}_m\right)$ defined by

$$\begin{pmatrix} \tilde{X}_m \\ \tilde{Y}_m \\ \tilde{Z}_m \end{pmatrix} = \begin{pmatrix} cos(\hat{\mu}_m) & sin(\hat{\mu}_m) & 0 \\ -sin(\hat{\mu}_m) & cos(\hat{\mu}_m) & 0 \\ 0 & 0 & 1 \end{pmatrix} \begin{pmatrix} X \\ Y \\ Z \end{pmatrix}, \tag{9}$$

(Fig. 8) each of which helps to define the half-plane H_m (Fig. 9), as follows:

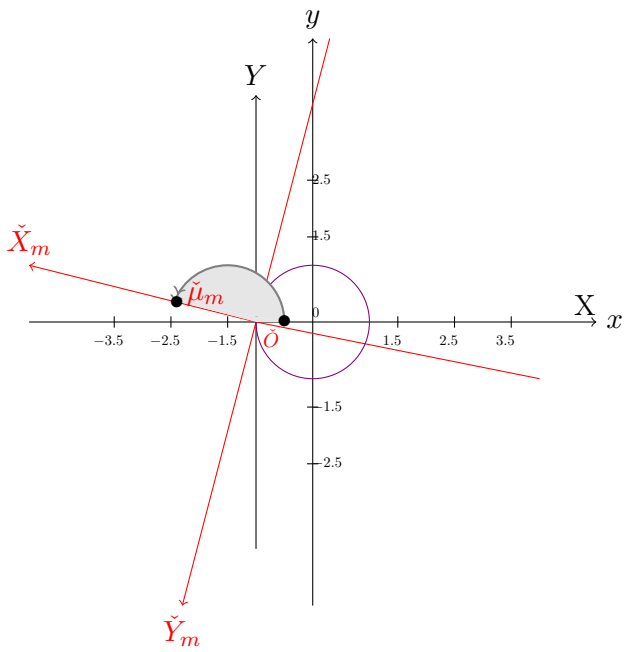

Figure 8. Systems of coordinates used to define the half-plane H_m

$$H_m = \left\{\tilde{X}_m \geq 0, \tilde{Y}_m = 0, \tilde{Z}_m \in \mathbb{R}\right\}. \tag{10}$$

On each half-plane H_m, the parabolic trajectory is parametrized by θ as

$$\begin{cases} \tilde{X}_m(\theta) = \beta_0\theta^2 + \gamma_0\theta + \delta_0, \\ \tilde{Z}_m(\theta) = \beta_1\theta + \gamma_1, \end{cases} \tag{11}$$

and verifies $\tilde{Z}_m(0) = z_m^r$, $\tilde{Z}_m(2T) = z_m^r - (2s+1)$ for the z-coordinate, and

$$\begin{cases} \tilde{X}_m(0) = 0, \\ \tilde{X}_m(T) = M, \\ \tilde{X}_m(2T) = 0, \end{cases} \tag{12}$$

for the x-coordinate (Fig. 9), where M is a constant defining the maximal amplitude of the parabola. Under those conditions, it is straightforward to obtain

$$\beta_0 = -\frac{M}{T^2}, \quad \gamma_0 = \frac{2M}{T}, \quad \delta_0 = 0 \quad \text{and} \quad \beta_1 = \frac{-(2s+1)}{2T}, \quad \gamma_1 = z_m^r, \tag{13}$$

$$\begin{cases} \tilde{X}_m(\theta) = \frac{M\theta}{T}\left(2 - \frac{\theta}{T}\right), \\ \tilde{Z}_m(\theta) = \frac{-(2s+1)}{2T}\theta + z_m^r. \end{cases} \tag{14}$$

Of course, the angle $\hat{\mu}_m$ must be bounded, for all the values of m. One can choose for example $\hat{\mu}_m = \frac{\pi}{8}(z_m^r - s) + \frac{15\pi}{16}$, which satisfies $\frac{15\pi}{16} < \hat{\mu}_m < \frac{17\pi}{16}$. The ribbon plotted in (Fig. 9) is defined with this value of $\hat{\mu}_m$, and $T = 1$, $s = 2$, $M = 2$.

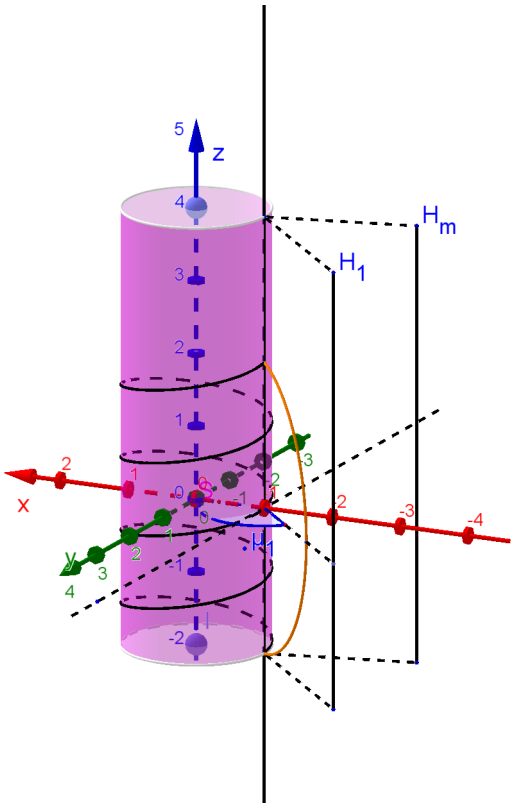

Figure 9. The dynamics of a neuron on the cylinder giving *spiking* and on the projection on H_1 giving the first period of quiescence, where the family $\{H_m\}_{m=0,\infty}$ is a sheaf of plane.

2.2.2. *The half-Poincaré map on the ribbon*

This second half-Poincaré map is defined, following the solution that starts from the reinjection interval until it reaches the injection interval.

Let $z_m^r \in I_s^r$. Considering $z(s) = (-2s - 1 + z_m^r) \in I_s^c$, set $z_{m+1}^c = (-2s - 1 + z_m^r)$. Then, define the map $\Psi_2 : I_s^r \longrightarrow I_s^c$ by $\Psi_2(z_m^r) = z(\tau_{m+1}^c) = z_{m+1}^c$, and

$$\Psi_2(z) = z - (2s + 1). \tag{15}$$

2.2.3. *Poincaré return map for a neuron*

The composition of both half-Poincaré maps Ψ_1 and Ψ_2 defines a Poincaré map $\Phi = \Psi_2 \circ \Psi_1$ on the reinjection interval. The map Ψ_1 is defined on I_s^c and takes values in I_s^r, and Ψ_2 takes values in I_s^c. Now, one has $\Phi_s : I_s^c \longrightarrow I_s^c$, where $\Phi_s = \Psi_2 \circ \Psi_1$ is given by

$$\Phi_s(z) = \begin{cases} z - 2s + [2s] + 1 & \text{for} \quad z \in [-s - 1, -s - 1 + \alpha[, \\ \\ z - 2s + [2s] & \text{for} \quad z \in [-s - 1 + \alpha, -s[. \end{cases}$$

By the change of coordinates, $\zeta = z + s + 1, \Phi(\zeta) = \Phi_s(z) + s + 1$, the map Φ_s is isomorphic to the map $\Phi : [0, 1[\to [0, 1[$, which is defined by

$$\Phi(\zeta) = \begin{cases} \zeta + 1 - \alpha & \text{for} \quad \zeta \in I_0, \\ \\ \zeta - \alpha & \text{for} \quad \zeta \in I_1, \end{cases} \tag{16}$$

with $\alpha = 2s - [2s]$, $I_0 = [0, \alpha[$, and $I_1 = [\alpha, 1[$.

Let $\zeta_0 \in [0, 1[$, and set $\zeta_0 = \Phi^0(\zeta_0)$ and $\zeta_m = \Phi^m(\zeta_0) \in [0, 1[$, for $m \geq 1$. The point $\Phi^m(\zeta_0) - (s + 1)$ denotes the position where the *bursting orbit* begins to turn around the cylinder to form the *burst* $B_{m_{(z_0)}}$ with $z_0 = \Phi^0(\zeta_0) - (s + 1)$.

It is equivalent to consider the *bursting* orbit $\mathcal{B}(z_0) = \{B_0(z_0), B_1(z_0), ..., B_m(z_0), ...\}$ or the *bursting* orbit of the Poincaré map $\Phi(\zeta_0) = \left\{\Phi^0(\zeta_0), \Phi^1(\zeta_0), ..., \Phi^m(\zeta_0), ...\right\}$.

From equation (5), it can be seen that the number of *spikes* within the *burst* B_m is $([2s] + 2)$ if $\Phi^m(\zeta_0)$ belongs to I_0 and $([2s] + 1)$ if $\Phi^m(\zeta_0)$ belongs to I_1.

An example of the distribution of *spikes* and quiescence regimes at a *burst* is illustrated by Fig. 10.

3. Periodic and quasi-periodic *bursting* orbits

In this section, the focus is on the number of *spikes* of each *burst* of a periodic *bursting* orbit.

Depending on the rationality or irrationality of the parameter α, the shape of the *burst* in such an orbit is quite different. There exist only periodic orbits for rational α, instead for irrational α, the model can have quasiperiodic orbits.

3.1. *Condition of existence of periodic bursting orbit*

Proposition 1. *If α is a rational number, $\alpha = \frac{p}{q}$, with $p, q \in N^*$, $0 < p < q$ and $pgcd(p, q) = 1$, then for any initial value $\zeta_0 \in [0, 1[$, the bursting orbit $\Phi(\zeta_0)$ is periodic of period q (i.e. $\Phi^q(\zeta_0) = \zeta_0$); moreover, q is the smallest possible period.*

Proof. For any initial condition $\zeta \in [0, 1[$, rewrite the map Φ as

$$\Phi(\zeta) = \zeta + \gamma \mod 1 \tag{17}$$

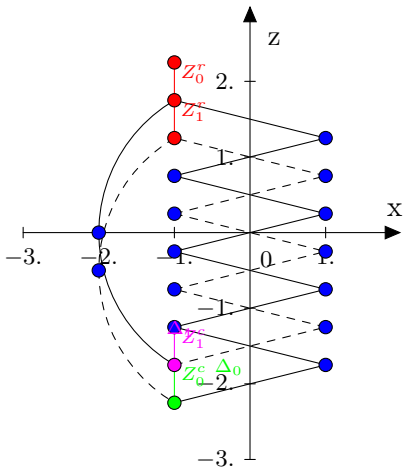

Figure 10. Plot of a *bursting* for $\alpha = \frac{1}{2}$

where $\gamma = 1 - \alpha$. Then, $\Phi^q(\zeta) = \zeta + q(1 - \frac{p}{q}) = \zeta + (q - p),\ (\text{mod } 1)$, hence $\Phi^q(\zeta) = \zeta$. ■

If q is not the smallest period, there exists a smallest period $\tilde{q}$ with $\tilde{q} < q$ and $q = n\tilde{q} + r$, where $r < \tilde{q}$. Then, $\zeta = \Phi^q(\zeta) = \Phi^{n\tilde{q}+r}(\zeta) = \Phi^r(\Phi^{n\tilde{q}})(\zeta) = \Phi^r(\zeta)$, which is impossible.

Remark 3.1. This is equivalent to that the corresponding orbit $\mathcal{B}(z_0)$ is periodic with q *bursts* belonging to the period.

Remark 3.2. It is important to point out the difference between the period of the *bursting* orbit $\Phi(\zeta_0)$ of the Poincaré map, which is an integer, and the period of the *bursting* orbit of the geometrical HR model, which is a duration T_s. In fact, even if q *bursts* are belonging to the period of the *bursting* orbit $\mathcal{B}(z_0)$, their periods can be different, depending on the value of $\alpha = \frac{p}{q}$. It will be proved bellow in Theorem 1 that $T_s = (2Tq + p([2s] + 2) + (q - p)([2s] + 1))$.

Remark 3.3. Two cylinders of nearly equal lengths can generate *bursting* orbits with a very different periods. As an example, for $s_1 = 1 + \frac{3}{5}$, the period is 5 while for $s_2 = 1 + \frac{3001}{5000}$ the period is 5000.

3.2. *Distribution of spikes and bursts in a periodic bursting orbit*

3.2.1. *Number of spikes and bursts*

Theorem 1. *For $\alpha = \frac{p}{q}$, a periodic bursting orbit with q bursts has p bursts of $([2s] + 2)$ spikes and $(q - p)$ bursts of $([2s] + 1)$ spikes.*

Therefore, the period of such orbit is equal to $T_s = (2Tq + p([2s] + 2) + (q - p)([2s] + 1))$.

In order to prove this theorem, define a partition of the interval I and prepare a lemma.

First, define $\triangle_j = [\frac{j}{q}, \frac{j+1}{q}[\subset I = [0, 1[,\ 0 \leq j \leq q - 1$. Thus, one can write $I_0 = \bigcup_{j=0}^{p-1} \triangle_j$ and $I_1 = \bigcup_{j=p}^{q-1} \triangle_j$. The intervals $\triangle_j$ form a partition of I and

$$\Phi(\triangle_j) = \begin{cases} \triangle_{j+(q-p)} \text{ when } \triangle_j \subset I_0 \ (j \leq p - 1), \\ \triangle_{j-p} \qquad \text{when } \triangle_j \subset I_1 \ (j \geq p). \end{cases} \tag{18}$$

Lemma 1.

- *For $m_1 \neq m_2$, $0 \leq m_i \leq q - 1$, $i = 1, 2$,*

$$\Phi^{m_1}(\triangle_j) \cap \Phi^{m_2}(\triangle_j) = \emptyset \quad \text{for all} \quad j, 0 \leq j \leq q - 1. \tag{19}$$

- *For $j_1 \neq j_2$, $0 \leq j_1, j_2 \leq q-1$,*

$$\Phi^m(\triangle_{j_1}) \cap \Phi^m(\triangle_{j_2}) = \emptyset \quad \textit{for all} \quad m. \tag{20}$$

Proof. [Proof of Lemma 1]

Suppose there exist $m_1 \leq q-1$ and $m_2 \leq q-1$, $m_1 < m_2$ such that $\Phi^{m_1}(\triangle_j) \cap \Phi^{m_2}(\triangle_j) \neq \emptyset$. Then, there exists $\triangle_l \subset \bigcup_{j=0}^{q-1} \triangle_j$ such that $\Phi^{m_1}(\triangle_j) = \triangle_l$ and $\Phi^{m_2}(\triangle_j) = \Phi^{(m_2-m_1)}(\Phi^{m_1}(\triangle_j)) = \Phi^{(m_2-m_1)}(\triangle_l) = \triangle_l$.

Thus, each point $\zeta \in \triangle_l$ is periodic with period $(m_2 - m_1) < q$. This contradicts the fact that $\Phi^q(\zeta) = \zeta$ for any $\zeta \in [0,1]$.

For the second case, it will be checked that if $j_1 \neq j_2$, then $\Phi(\triangle_{j_1}) \cap \Phi(\triangle_{j_2}) = \emptyset$.

Indeed, for $j_1 \neq j_2$, if $\triangle_{j_1}$ and $\triangle_{j_2}$ belong to I_0 then $\Phi(\triangle_{j_i}) = \triangle_{j_i} + (q-p)$ for $i = 1, 2$ and $j_1 + (q-p) \neq j_2 + (q-p)$.

One also has $\Phi(\triangle_{j_i}) = \triangle_{j_i} - p$, $i = 1, 2$ and $j_1 - p \neq j_2 - p$ if $\triangle_{j_1}$ and $\triangle_{j_2}$ belong to I_1 and so $\Phi(\triangle_{j_1}) \cap \Phi(\triangle_{j_2}) = \emptyset$.

In the case where $\triangle_{j_1} \subset I_0$ and $\triangle_{j_2} \subset I_1$, one has $\Phi(\triangle_{j_1}) = \triangle_{j_1} + (q-p)$ and $\Phi(\triangle_{j_2}) = \triangle_{j_2} - p$. Suppose that $\Phi(\triangle_{j_1}) \cap \Phi(\triangle_{j_2}) \neq \emptyset$. From (21), this implies that $\Phi(\triangle_{j_1}) = \Phi(\triangle_{j_2})$, that is $\triangle_{j_1} + (q-p) = \triangle_{j_2} - p$, which is impossible since $j_2 \leq q-1$.

The case of $\triangle_{j_1} \subset I_1$ and $\triangle_{j_2} \subset I_0$ is the same as this last one.

Therefore, for all m, $\Phi^m(\triangle_{j_1}) \cap \Phi^m(\triangle_{j_2}) = \emptyset$ if $j_1 \neq j_2$. ■

Remark 3.4. Lemma 1 implies that

- For each $\triangle_j \subset \bigcup_{i=0}^{q-1} \triangle_i$, $(\Phi^0(\triangle_j), \Phi^1(\triangle_j), ..., \Phi^{q-1}(\triangle_j))$ are disjoint sets, so

$$\bigcup_{m=0}^{q-1} \Phi^m(\triangle_j) = \bigcup_{j=0}^{q-1} \triangle_j = [0,1[.$$

- Let $\zeta_0 \in \triangle_j$. Then, $(\zeta_0, \Phi^1(\zeta_0), ..., \Phi^{q-1}(\zeta_0)) \in (\triangle_j, \Phi^1(\triangle_j), ..., \Phi^{q-1}(\triangle_j))$, i.e. for $\zeta_0 \in \triangle_j$, $\Phi^m(\zeta_0) \in \Phi^m(\triangle_j)$, for $0 \leq m \leq q-1$. Thus,

$$\bigcup_{m=0}^{q-1} \Phi^m(\triangle_j) = \left(\bigcup_{j=0}^{p} \triangle_j \right) \bigcup \left(\bigcup_{j=p+1}^{q-1} \triangle_j \right) = I_0 \bigcup I_1.$$

Therefore, there are p iterations on I_0 and $(q-p)$ iterations on I_1.

Lemma 1 and remarks 3.4 complete the proof of Theorem 1.

Hence, the lenght T_s of this period is established.

3.2.2. *Equivalent bursting orbits*

Definition 3.1. Two periodic *bursting* orbits are called equivalent if their trajectories have the same period T_s and differ from each other by only a translation.

In terms of *bursting* orbit of a Poincaré map, two orbits are said to be equivalent if they have the same period q, with $\alpha = \frac{p}{q}$, and differ from each other up to a phase shift. It means that one could put the initial condition anywhere on the intervall $[0,1[$ and obtain equivalent orbits.

Now, define a matrix $A = (a_{mj})_{0 \leq m,j \leq q-1}$, where a_{mj} is the index of the interval $\triangle_{a_{mj}}$, i.e. $\Phi^m(\triangle_j) = \triangle_{a_{mj}}$. The elements of the column j are indices of the intervals $(\triangle_j, 0 \leq j < q)$ and the elements of the row are the numbers of the iterations of the orbits. It follows from Lemma 1 that

(1) If $a_{m_1 j} = a_{m_2 j}$, then $m_1 = m_2$.
(2) If $a_{m j_1} = a_{m j_2}$, then $j_1 = j_2$.

Lemma 2. *For $n < q$, one has*

$$\Phi^n(\triangle_j) = \begin{cases} \triangle_{j+n(q-p)} & if\ \triangle_{j+m(q-p)} \subset I_0, m = 0, ..., n-1, \\ \triangle_{j+(n-l)(q-p)-lp}, (l = 1, ..., n-1) & if\ \triangle_{a_{mj}} \subset I_k, k = 0 \quad or \quad 1, \\ \triangle_{j-np} & if\ \triangle_{j-mp} \subset I_1, m = 0, ..., n-1. \end{cases}$$

where $\triangle_{a_{mj}}$ is of the form $\triangle_{j+m_1(q-p)-m_2p}$ and $m_1 = 0, ..., n-1, m_2 = 0, ..., n-1$.

One can easily prove this lemma by induction and show that $\Phi^n(\triangle_j) = \triangle_{j+(n-l)(q-p)-lp}$ holds for $l = 0, ..., n$, and $n < q$.

Next, it will show how the distribution of *bursts* takes place along a *bursting* orbit.

The following proposition proves that $\Phi^m(\triangle_i)$ and $\Phi^m(\triangle_j)$, for $i \neq j$, do not bounce in the same way around I_0 and I_1, and gives the repartion of the *bursts* in an orbit.

Proposition 2. *For each $i < q$ and for each $j < q$, with $i \neq j$, there is n, $n < q$, such that $\Phi^n(\triangle_i)$ lies in I_0 and $\Phi^n(\triangle_j)$ lies in I_1, or $\Phi^n(\triangle_i)$ lies in I_1 and $\Phi^n(\triangle_j)$ lies in I_0. Furthermore, there are exactly q bursting orbits $(\zeta_0, \Phi^1(\zeta_0), ..., \Phi^{q-1}(\zeta_0))$, $\zeta_0 \in \triangle_j$, which are equivalent to each other.*

Proof. In the case where $\triangle_i$ and $\triangle_j$ do not belong to the same interval I_0 or I_1, that is, $i < p$ and $j \geq p$, take $n = 0$.

In the case where $\triangle_i$ and $\triangle_j$ belong to the same interval, say I_0, suppose $\Phi^m(\triangle_i) = \triangle_{a_{mi}}$ and $\Phi^m(\triangle_j) = \triangle_{a_{mj}}$ lie in the same interval I_0. Then, from lemma 2, one has $(a_{mj} - a_{mi}) = (j - i)$ for $m < q$.

It follows that $\Phi^m(\triangle_i)$ and $\Phi^m(\triangle_j)$ can only visit $(p - (j - i))$ times the interval I_0. This contradicts the fact that $\Phi^m(\triangle_i) = \triangle_{a_{mi}}$ visits p times the interval I_0 for $m < q$.

One can show in the same manner that there is n such that $\Phi^n(\triangle_i) \in I_1$ and $\Phi^n(\triangle_j) \in I_0$. ■

Remark 3.5. In the above, it has been proved that there is n_0 such that $\Phi^{n_0}(\triangle_i) \in I_0$ and $\Phi^{n_0}(\triangle_j) \in I_1$. In this case, there should be an n_1 such that $\Phi^{n_1}(\triangle_i) \in I_1$ and $\Phi^{n_1}(\triangle_j) \in I_0$. If not, then $\Phi^m(\triangle_i)$ and $\Phi^m(\triangle_j)$ are in the same interval, I_0 or I_1, with $m \neq n_0$. Suppose they are in I_0. Then, for $m \neq n_0$, each of $\Phi^m(\triangle_i)$ and $\Phi^m(\triangle_j)$ visits p times the interval I_0. Since $\Phi^{n_0}(\triangle_i)$ is in I_0, $\Phi^m(\triangle_i)$ visits $(p + 1)$ times the interval I_0 for all $m < q$. This contradicts the fact that $\Phi^m(\triangle_i)$ visits p times the interval I_0 for $m < q$.

The number of indices n_i is an even number.

3.2.3. *Repartition of spikes and bursts in a periodic bursting orbit*

Let r be the residual of euclidian division of $(q - p)$ by p if $(q - p) > p$, or the residual of euclidian division of p by $(q - p)$ if $(q - p) < p$. Then, the repartition of the *bursts* in a *bursting* orbit is performed in the following way:

Theorem 2.

- *If $(q-p) > p$, i.e. $|I_1| > |I_0|$, then the $(q-p)$ bursts of $([2s]+1)$ spikes are distributed in p sets of repetitive bursts of $([2s]+1)$ spikes, separated by bursts of $([2s]+2)$ spikes. In these p sets, there are $(p-r)$ sets of $n = [\frac{q-p}{p}]$ repetitive bursts of $([2s]+1)$ spikes and r sets of $(n+1)$ repetitive bursts of $([2s]+1)$ spikes.*

- *If $(q-p) < p$, then the p bursts are distributed in $(q-p)$ sets of repetitive bursts of $([2s]+2)$ spikes, separated by bursts of $([2s]+1)$ spikes. In these $(q-p)$ sets, there are $(q-p-r)$ sets of $n = [\frac{p}{q-p}]$ repetitive bursts of $([2s]+2)$ spikes and r sets of $(n+1)$ repetitive bursts of $([2s]+2)$ spikes.*
- *If $(q-p) = p$, i.e. $q = 2p$ and $\alpha = 1/2$, then the periodic bursting orbits are of the form: $([2s]+1)$ $([2s]+2)$, which can be repeated periodically.*

Proof. For $\alpha = p/q$, a *bursting* orbit has p *bursts* of $([2s]+2)$ *spikes* and $(q-p)$ *bursts* of $([2s]+1)$ *spikes*. If $(q-p) > p$, then from euclidian division one can write $(q-p) = p[\frac{q-p}{p}] + r = (p-r)n + r(n+1)$, where $n = [\frac{q-p}{p}]$. So, the $(q-p)$ *bursts* of $([2s]+1)$ *spikes* are distributed in $(p-r)$ sets of n *bursts* and r sets of $(n+1)$ *bursts*.

In addition, for any i, since $p < (q-p)$, if $\Phi^i(\triangle_j) \in I_0$, then $\Phi^{i+1}(\triangle_j) = \triangle_{j+(q-p)} \in I_1$. Thereby, each time when the trajectory passes through the I_0 interval, it leaves this interval at the next iteration, thus generating a single *burst* of $([2s]+2)$ *spikes*. The same reasoning applies if $(q-p) < p$.

In the case of $(q-p) = p$, one has

$$\Phi(\triangle_j) = \begin{cases} \triangle_{j+p} \text{ when } \triangle_j \subset I_0 \ (j \leq p-1), \\ \\ \triangle_{j-p} \text{ when } \triangle_j \subset I_1 \ (j \geq p). \end{cases} \tag{21}$$

So, if $\triangle_j \in I_0$ then $\Phi(\triangle_j) = \triangle_{j+p} \in I_1$ and $\Phi^2(\triangle_j) = \triangle_j \in I_0$.

In the same way, if $\triangle_j \in I_1$ then $\Phi(\triangle_j) = \triangle_{j-p} \in I_0$ and $\Phi^2(\triangle_j) = \triangle_j \in I_1$. Therefore, the *bursting* orbits are of the form: $([2s]+1)\ ([2s]+2)$, or equivalently, $([2s]+2)\ ([2s]+1)$. ■

Fig. 11 depicts a periodic *bursting* trajectory computed for $s = 1.3$ and $\alpha = \frac{3}{5}$ with periodic pattern of the form (44343). In this case, $(q-p) < p$, $n = 1$ and $r = 1$. So, as can be observed in Fig. 11, there are a set of $(n+1) = 2$ *bursts* of 4 *spikes* and a set of $n = 1$ *burst* of 4 *spikes*, each of which is separated by a *burst* of 3 *spikes*.

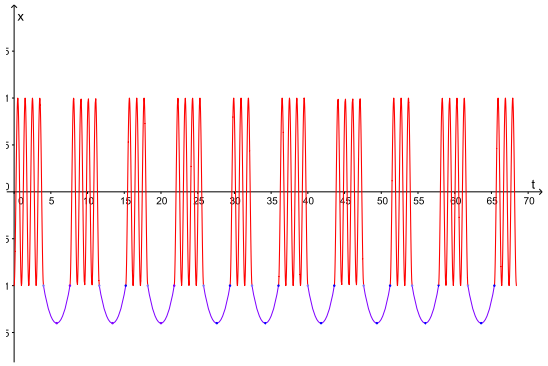

Figure 11. *Bursting* trajectory with (44343) pattern for $\alpha = \frac{3}{5}$ and $s = 1.3$

.

The next two theorems give the form of the *bursting* according to whether $p-r > r$, $p-r < r$ or $p-r = r$, with a specific case of $p-r = 1$.

Theorem 3.

(1) For $\zeta_0 \in \triangle_{q-1}$, if $p-r > r$, the periodic bursting is distibuted in the following way:

$$\underbrace{U...U}_{n+1}W \quad \underbrace{\underbrace{U...U}_{n}W...\underbrace{U...U}_{n}W}_{n(0)} \quad \underbrace{U...U}_{n+1}W \quad \underbrace{\underbrace{U...U}_{n}W...\underbrace{U...U}_{n}W}_{n(1)} \quad ... \quad \underbrace{U...U}_{n+1}W \quad \underbrace{\underbrace{U...U}_{n}W...\underbrace{U...U}_{n}W}_{n(i)} \tag{22}$$

where $U = [2s]+1$, $W = [2s]+2$, $p-r = n(0)r + r(0)$, $p-(r-r(0)) = n(1)r + r(1)$, $p-(r-r(1)) = n(2)r + r(2)$,..., $p-(r-r(i-1)) = n(i)r + r(i)$, with $n(0)+n(1)+...+n(i) = p-r$ if $r(i) = 0$.

(2) For $\zeta_0 \in \triangle_{q-1}$, if $p-r<r$, the periodic bursting is distributed in the following way:

$$\underbrace{\underbrace{U...U}_{n+1}W...\underbrace{U...U}_{n+1}W}_{n(0)+1}\quad\underbrace{\underbrace{U...U}_{n}W}_{n}\quad\underbrace{\underbrace{U...U}_{n+1}W...\underbrace{U...U}_{n+1}W}_{n(1)+1}\quad\underbrace{\underbrace{U...U}_{n}W}_{n}\quad ...\quad\underbrace{\underbrace{U...U}_{n+1}W...\underbrace{U...U}_{n+1}W}_{n(i)+1}\quad\underbrace{\underbrace{U...U}_{n}W}_{n} \tag{23}$$

where $r-1=n(0)(p-r)+r(0)$, $r-(p-r)+r(0)=n(1)(p-r)+r(1)$,..., $r-(p-r)+r(i-1)=n(i)(p-r)+r(i)$ and $(n(0)+1)+...+(n(i-1)+1)=r$ if $r(i)=0$ for $i\neq 0$.

Proof. First, perform a *bursting* for an initial condition $\zeta_0 \in \triangle_{q-1}$. For the other initial conditions, from Proposition 2, the other periodic *bursting* are equivalent to this one.

Then, recall that for any i, since $p<(q-p)$, if $\Phi^i(\triangle_j)\in I_0$, then $\Phi^{i+1}(\triangle_j)=\triangle_{j+(q-p)}\in I_1$.

(1) If $p-r>r$ i.e. $p>2r$, then for $\zeta_0\in\triangle_{q-1}$ one has

$$\Phi^{(n+1)}(\triangle_{q-1})=\triangle_{r-1}=\Big[\frac{r-1}{q},\frac{r}{q}\Big[\subset\Big[\frac{r-1}{q},\frac{p-r}{q}\Big[\subset I_0, \tag{24}$$

$$\Phi^{(n+1)+1}(\triangle_{q-1})=\triangle_{np+2r-1}=\Big[\frac{np+2r-1}{q},\frac{np+2r}{q}\Big[\subset\Big[\frac{p}{q},\frac{(n+1)p}{q}\Big[\subset I_1 \tag{25}$$

$$\text{since}\quad np+2r<np+p. \tag{26}$$

Let $p-r=n(0)r+r(0)$. Then,

$$\Phi^{[(n+1)+1]+n(0)n+n(0)}(\triangle_{q-1})=\triangle_{np+2r-1+n(0)r}=\triangle_{(n+1)p+r-r(0)-1}=\triangle_{q-1-r(0)}\quad(r>r(0)). \tag{27}$$

Putting $\tilde{n}=[(n+1)+1]+n(0)n+n(0)$, one obtains

$$\Phi^{\tilde{n}}(\triangle_{q-1})=\triangle_{q-1-r(0)}. \tag{28}$$

Thus, the first part of the *bursting* is given by

$$\underbrace{\underbrace{U...U}_{n+1}W\underbrace{\underbrace{U...U}_{n}W...\underbrace{U...U}_{n}W}_{n(0)}}$$

For the next iterations, one has

$$\Phi^{\tilde{n}+(n+1)}(\triangle_{q-1})=\triangle_{r-r(0)-1}\subset I_0,$$

and

$$\Phi^{\tilde{n}+(n+1)+1}(\triangle_{q-1})=\triangle_{np+2r-r(0)-1}=\triangle_{(n+1)p+r-1-(p-(r-r(0)))}=\triangle_{(n+1)p+r-1-n(1)r-r(1)}, \tag{29}$$

where $p-(r-r(0))=n(1)r+r(1)$. So,

$$\Phi^{\tilde{n}+(n+1)+1+n(1)n+n(1)}(\triangle_{q-1})=\triangle_{(n+1)p+r-r(1)-1}. \tag{30}$$

Let $\tilde{m}=\tilde{n}+(n+1)+1+n(1)n+n(1)$. Then,

$$\Phi^{\tilde{m}}(\triangle_{q-1})=\triangle_{q-1-r(1)}. \tag{31}$$

Therefore, the next part of the *bursting* is

$$\underbrace{\underbrace{U...U}_{n+1}W\underbrace{\underbrace{U...U}_{n}W...\underbrace{U...U}_{n}W}_{n(1)}}.$$

Now, from (40), one can repeat the process as for (28) to obtain the complete periodic *bursting*.

(2) If $p-r<r$ i.e. $p<2r$, then for $\zeta_0\in\triangle_{q-1}$, one has

$$\Phi^{(n+1)}(\triangle_{q-1})=\triangle_{r-1}=\Big[\frac{r-1}{q},\frac{r}{q}\Big[\subset\Big[\frac{r-1}{q},\frac{p-r}{q}\Big[\subset I_0, \tag{32}$$

$$\Phi^{(n+1)+1}(\triangle_{q-1})=\triangle_{np+2r-1}\subset\Big[\frac{(n+1)p}{q},\frac{(n+1)p+r}{q}\Big[\subset I_1, \tag{33}$$
$$\text{since}\quad np+2r-1>np+p-1.$$

So,

$$\Phi^{(n(0)+1)(n+1)+n(0)+1}(\triangle_{q-1})=\triangle_{np+r-1-n(0)(p-r)+r}. \tag{34}$$

Let $r-1=n(0)(p-r)+r(0)$ with $r(0)<r$. Then,

$$\Phi^{(n(0)+1)(n+1)+n(0)+1}(\triangle_{q-1})=\triangle_{np+r+r(0)}\subset\Big[\frac{p}{q},\frac{(n+1)p}{q}\Big[\quad\text{since}\quad r(0)<r, \tag{35}$$

and

$$\Phi^{\tilde{n}}(\triangle_{q-1})=\triangle_{np+r+r(0)}, \tag{36}$$

for $\tilde{n}=(n(0)+1)(n+1)+n(0)+1$. The first part of the periodic *bursting* is then given by

$$\underbrace{\underbrace{U...U}_{n+1}W...\underbrace{U...U}_{n+1}W}_{n(0)+1}. \tag{37}$$

For the next, one has

$$\Phi^{\tilde{n}+n+1}(\triangle_{q-1})=\triangle_{(n+1)p+r-(p-r)+r(0)}=\triangle_{(n+1)p+n(1)(p-r)+r(1)}, \tag{38}$$

where $n(1)$ and $r(1)$ are defined by $r-(p-r)+r(0)=n(1)(p-r)+r(1)$. Then,

$$\Phi^{\tilde{n}+n+1+(n(1)+1)(n+1)+n(1)+1}(\triangle_{q-1})=\triangle_{(n+1)p-(p-r)+r(1)}=\triangle_{np+r+r(1)}. \tag{39}$$

Putting $\tilde{m}=\tilde{n}+n+1+(n(1)+1)(n+1)+n(1)+1$, one obtains

$$\Phi^{\tilde{m}}(\triangle_{q-1})=\triangle_{np+r+r(1)}. \tag{40}$$

So, the next part of the *bursting* is

$$\underbrace{\underbrace{U...U}_{n}W\underbrace{U...U}_{n+1}W...\underbrace{U...U}_{n+1}W}_{n(1)+1} \tag{41}$$

Then, from (40), one can repeat the precedent process to give the complete periodic *bursting*.

■

As an example, consider the following two cases:

(1) For $p=7$, $q=17$, there are 7 *busts* of 4 *spikes* and $q-p=10$ *bursts* of 3 *spikes*, $n=1$, $r=3$, $p-r=4>r$, $r(0)=1$, $n(0)=n(1)=1$, $r(1)=2$, $n(2)=2$ and $r(2)=0$. Thus, the periodic *bursting* is given by (33433433433433433) (see Fig. 12).
(2) For $p=5$, $q=13$, there are 5 *bursts* of 4 *spikes* and $q-p=8$ *bursts* of 3 *spikes*, $n=1$, $r=3$, $p-r=2<r$, $n(0)=1$, $r(0)=0$, $n(1)=0$, $r(1)=1$, $n(2)=0$ and $r(2)=0$. The *bursting orbit* has the pattern (3343343433434) (see Fig. 13).

Remark 3.6. For the case of $p-r=r$, i.e. $p=2r$, $q=(n+1)p+r=(2n+3)r$ and $pgcd(p,q)=r\neq 1$ for $r\neq 1$. If $r=1$, then the case of $p-r=r$ is included in the general case of $p=r+1$.

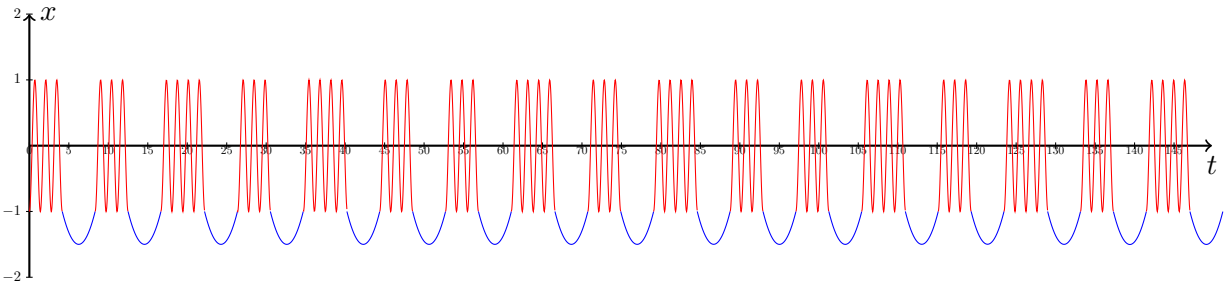

Figure 12. *Bursting* trajectory with (33434334343343434) pattern for $\alpha = 7/17$ and $p - r > r$

.

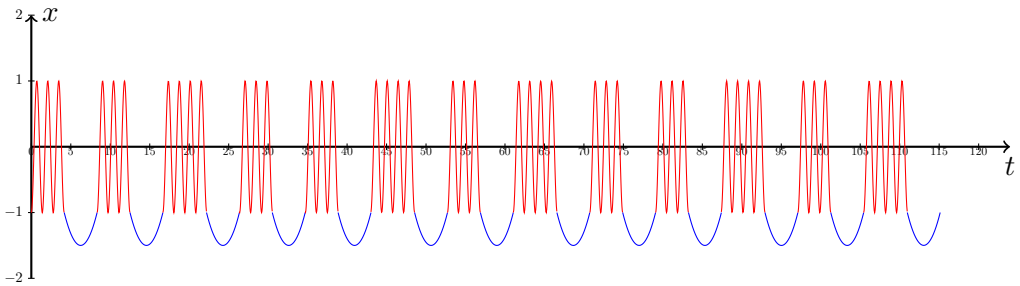

Figure 13. *Bursting* trajectory with (3343343433434) pattern for $\alpha = 5/13$ and $p - r < r$

.

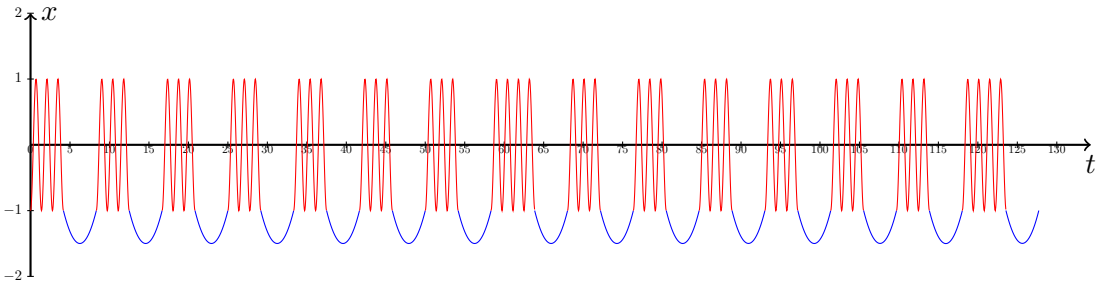

Figure 14. *Bursting* trajectory with (333333343333334) pattern for $\alpha = 2/15$ and $p = r + 1$

.

Theorem 4. *For $\zeta_0 \in \triangle_{q-1}$, if $p = r + 1$, then the periodic bursting is distributed in the following way:*

$$\underbrace{\underbrace{\underbrace{U...U}_{n+1}W\underbrace{U...U}_{n+1}W}_{r}\quad\underbrace{\underbrace{U...U}_{n}W\underbrace{U...U}_{n}W}_{(p-r)}}_{} \tag{42}$$

Proof. For $\zeta_0 \in \triangle_{q-1}$, one has

$$\Phi^{(n+1)}(\triangle_{q-1}) = \triangle_{r-1} \subset I_0, \tag{43}$$

and

$$\Phi^{r(n+1)+r}(\triangle_{q-1}) = \triangle_{(n+1)p+r-1-r(p-r)} = \triangle_{(n+1)p-1} = \triangle_{np+r} \subset I_1. \tag{44}$$

Thus, the first part of the *bursting* is

$$\underbrace{\underbrace{U...U}_{n+1}W...\underbrace{U...U}_{n+1}W}_{r} \tag{45}$$

Next, let $\tilde{n} = r(n+1)+r$. Then,

$$\Phi^{\tilde{n}+n(p-r)+(p-r)}(\triangle_{q-1}) = \triangle_{(n+1)p+r-1} = \triangle_{q-1}. \tag{46}$$

So, the $p-r$ remaining *bursts* are distributed in the following way:

$$\underbrace{\underbrace{U...U}_{n}W...\underbrace{U...U}_{n}W}_{p-r} \tag{47}$$

■

Consider an example for this case. For $p=2$, $q=15$, there are 2 *busts* of 4 *spikes* and $q-p=13$ *bursts* of 3 *spikes*, $n=6$, $r=1$, $p-r=1$. Thus, the periodic *bursting* is (333333343333334) (see Fig. 14).

3.3. *Quasi-periodic bursting orbits*

When α is an irrational number, since the application of Φ is the translation $\zeta \to \zeta+\alpha \pmod 1$, each orbit is everywhere dense. Each point in $[0,1[$ has an infinite orbit and at each iteration a new point reaches on the interval $[0,1[$ so giving rise to a "uniform distribution" on the interval, in the sens that these points are landing, in an ordered manner, in $I_0=[0,\alpha[$ or $I_1=[\alpha,1[$, depending on whether they belong to either of the two intervals. No point is ever revisited in finite time, thus each orbit consists of a quasi periodic *bursting*.

Let I be an interval $\in [0,1[$ and $F(x,n) = \#\left\{1 \le k \le n/\Phi^k(x) \in I\right\}$, where "#" denotes the number of elements in a set. Then, from Weyl's Theorem [H. Weyl, 1916] below, for n large enough, the average number of points lying in the interval I is equal to the length of this interval. Hence, for each x in $[0,1[$, the iterations $\Phi^n(x)$ are uniformly distributed (mod 1), that is, the proportion of points lying in the intervals I_0 and I_1 is respectively α and $1-\alpha$.

Theorem 5. *(Weyl 1916) Let I be an interval of the form $[c,d]$, with $0 \le c < d \le 1$. Then, one has $lim_{n\to+\infty}\frac{F(x,n)}{n} = c-d$*

Fig. 15 and Fig. 16 show respectively the iterates of the map Φ with the irrational number $\alpha=\frac{1}{\pi}$ and $\alpha=\frac{1}{\sqrt{2}}$. The red circle represents the *burst* of ([2s]+1) *spikes* and the blue one the *burst* of ([2s]+2) *spikes*. The number n below or above each circle represents the n-th *burst*.

It can be observed that, when the number of iterations increases, the distance between two *bursts* decreases and the *bursts* become closer and closer to each other (see for instance *bursts* 2 and 24 in Fig. 15 and *bursts* 7 and 48 in Fig. 16).

When the number of iteration increases, the *burst* of ([2s]+1) spikes will fill up all the interval I_1 and the one of ([2s]+2) *spikes* will fill up all the interval I_0.

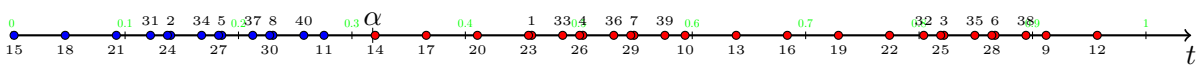

Figure 15. Irrational *bursting* trajectory for $\alpha = 1/\pi$

.

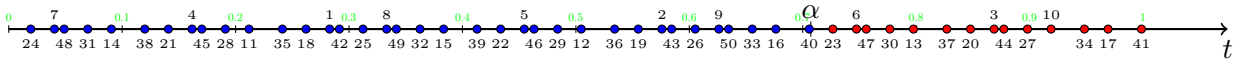

Figure 16. Irrational *bursting* trajectory for $\alpha = 1/\sqrt{2}$

.

4. Chaotic *bursting* oscillations

Dynamics on the ribbon is a key to shape the nature of solutions. Comparing Fig. 1 and Fig. 2, it is obvious that, on the ribbon, solutions are spreading in different ways before reaching the cylinder.

Now, consider the dynamics different from those defined in Sec. 2, which allows the onset of chaotic *bursting* oscillations. These chaotic *bursting* orbits display mixing of *bursts* with U and W *spikes*.

4.1. *Chaotic dynamics on the ribbon*

Keeping the same notation of Sec. 2, on each half-plane H_m, the parabolic trajectory parametrized by θ is given by

$$\begin{cases} \tilde{X}_m(\theta) = \frac{M\theta}{T}(2-\theta), \\ \tilde{Z}_m(\theta) = -\frac{(2s+1)}{2T}\theta - 2z_m^r + 3s + 1 \quad \text{for} \quad z_m^r \in [s, s+\frac{1}{2}[, \\ \tilde{Z}_m(\theta) = -\frac{(2s+1)}{2T}\theta + 2z_m^r - s - 1 \quad \text{for} \quad z_m^r \in [s+\frac{1}{2}, s+1[. \end{cases} \tag{48}$$

4.2. *Poincaré return map*

The half-Poincaré map Ψ_2 on the ribbon is the symmetric tent map. Then, the map $\Phi = \Psi_2 \circ \Psi_1$ is given by

If $\alpha \leq \frac{1}{2}$,

$$\Phi(\zeta) = \begin{cases} -2\zeta + 2\alpha & if\ \zeta \in [0, \alpha[, \\ 2\zeta - 2\alpha & if\ \zeta \in [\alpha, \alpha + \frac{1}{2}[, \\ -2\zeta + 2\alpha + 2 & if\ \zeta \in [\alpha + \frac{1}{2}, 1[. \end{cases} \tag{49}$$

(see Fig. 17).

If $\alpha \geq \frac{1}{2}$,

$$\Phi(\zeta) = \begin{cases} 2\zeta + 2(1-\alpha) & if\ \zeta \in [0, \alpha - \frac{1}{2}[, \\ -2\zeta + 2\alpha & if\ \zeta \in [\alpha - \frac{1}{2}, \alpha[, \\ 2\zeta - 2\alpha & if\ \zeta \in [\alpha, 1[. \end{cases} \tag{50}$$

(see Fig. 20).

This proves that Φ has a horseshoe on the interval I.

Let J be a closed interval of I. Suppose that there are two disjoint closed intervals, $K_0 \subset J \cap I_0$ and $K_1 \subset J \cap I_1$, and the restriction of Φ to each K_i, i.e., $\Phi|K_i$, is monotonic and continuous, such that $\Phi(K_j) \supset \cup_{i=0}^{1} K_i$, $j = 0, 1$.

Let

$$\Sigma = \{(t_0, t_1, t_2, \cdots), t_j = 0 \quad \text{or} \quad t_j = 1\},$$
$$\Lambda = \{\zeta \in I : \Phi^n(\zeta) \in I \quad \forall n \geq 0\},$$

and the shift map $\sigma : \Sigma \to \Sigma$ defined by $\sigma(t_0 t_1 t_2 \cdots) = (t_1 t_2 t_3 \cdots)$.

Recall ([Devaney, 2003]) that there exists a compact invariant set $\Lambda \subset J$, such that $\Phi|\Lambda$ is semi-conjugate to the shift map σ on Σ via a continuous and onto map $h : \Sigma \longrightarrow \Lambda$, where

$$\Lambda = \cap_{i=0}^{\infty}\Phi^{-i}(K_1 \cup K_0) = \cup_{(t_0t_1t_3\cdots)\in\Sigma} \cap_{i=0}^{\infty} \Phi^{-i}(K_{t_i}). \tag{51}$$

One has

$$\Phi^n \circ h = h \circ \sigma^n.$$

So, h converts $\sigma-$orbits to $\Phi-$orbits. Therefore, $\Phi-$orbits are in one$-$to$-$one correspondence with $\sigma-$orbits. In particular, if t is a periodic point for σ, then $h(t)$ is a periodic point for Φ with the same period. If there is an eventually periodic point for σ, then h gives an analogous point for Φ. Indeed, h converts the dynamical behavior observed for σ. Thus, the dynamics of σ on Σ and Φ on Λ are essentially the same.

For any $\zeta_0 \in \Lambda$, there is $t_0 = (t_0(0)t_0(1)t_0(2)\cdots) \in \Sigma$ such that $\Phi^{n-1}(\zeta_0) \in K_{t_0(n-1)} \subset I_{t_0(n-1)}$. The point $(\Phi^n(\zeta_0) - (2s+1))$ denotes the point where the *bursting* orbit begins to turn around the cylinder to form the *burst* B_n. The number of *spikes* within the *burst* B_n is

$$t_0(n-1)(2[s]+1) + (1 - t_0(n-1))([2s]+2)),$$

that is, the number of *spikes* within the *burst* B_n is $([2s]+2)$ if $\Phi^{n-1}(\zeta_0)$ lies in K_0 $(t_0(n-1) = 0)$ and $([2s]+1)$ if $\Phi^{n-1}(\zeta_0)$ lies in $K_1(t_0(n-1) = 1)$.

The map σ has countably infinitely many of periodic orbits consisting of the orbits of all periods, and for any $n > 0$, σ has $(2^n - 2)$ periodic points of period n.

Let $t_i = (t_i(0)t_i(1)\cdots t_i(n-1)t_i(0)t_i(1)\cdots t_i(n-1)\cdots)$ be a periodic point of period n for σ. Then, there is $\zeta_0 \in \Lambda$ such that $h(t_i) = \zeta_0$ is a periodic point of period n for Φ with $\Phi^m(\zeta_0) \in K_{t_i(m)}$ for any $m < n$ and $\Phi^n(\zeta_0) = \zeta_0 \in K_{t_i(0)}$. There is a *bursting* orbit of period

$$T_i = a_i([2s]+2) + b_i([2s]+1) + \sum_{j=0}^{n-1} \beta_{i,j},$$

with $a_i + b_i = n$, where $a_i = \sharp\{j \leq n-1, t_i(j) = 0\}$ is the number of *bursts* of $([2s]+2)$ *spikes* and $b_i = \sharp\{j \leq n-1, t_i(j) = 1\}$ is the number of *bursts* of $([2s]+1)$ *spikes*, and $\beta_{i,j}$ denotes the time it takes for the solution to form the period of quiescence $j < n-1$ and then return to the cylinder.

Therefore, for each period n of σ, there are $(2^n - 2)$ types of periodic *bursting* of periods T_i, $1 \leq i \leq (2^n - 2)$, with all possible distributions of numbers of *spikes* $([2s]+2)$ and $([2s]+1)$ per *bursts*.

Proposition 3. *For $\alpha < \frac{1}{2}$, Φ has horseshoes on the intervals $[0, 2\alpha]$ and $[2\alpha, 1]$. In the interval $[0, 2\alpha]$, there are $K_0 = [0, \alpha] \in I_0$ and $[\alpha, 2\alpha] \in I_1$ and $\Phi([0, 2\alpha]) = [0, 2\alpha]$, and in the interval $[2\alpha, 1]$, $\Phi([2\alpha, 1]) = [2\alpha, 1]$.*

In the case of $\alpha > \frac{1}{2}$, for $\alpha = 0.75$, Φ^2 has a horseshoe on the interval $[0, 0.5]$ with $\Phi^2([0, 0.5]) \subset [0, 0.5] \subset I_0$ and a horseshoe on the interval $[0.5, 1]$ with $\Phi^2([0.5, 1]) \subset [0.5, 1]$.

Remark 4.1. For $\alpha < \frac{1}{2}$, for initial conditions in the interval $[0, 2\alpha]$, there are *burstings* with a mix of $(2[s]+1)$ and $([2s]+2)$ *bursts* (see Fig. 18). For initial conditions in the interval $[2\alpha, 1] \subset I_1$, there is *bursting* with only $(2[s]+1)$ *bursts* (see Fig. 19).

For $\alpha = 0.75$, $\Phi^2([0, 0.5]) \subset I_0$, so there is *bursting* with only $([2s]+2)$ *bursts* (see Fig. 21) and in the interval $[0.5, 1]$, there is *bursting* with a mix of (2[s]+1) and ([2s]+2) *bursts* (see Fig. 22).

Proof. For $\alpha < \frac{1}{2}$ (see Fig. 17 for $\alpha = 1.8$), one has $\Phi(2\alpha) = 2\alpha$, so $\Phi([0, 2\alpha]) = [0, 2\alpha]$ and $\Phi([2\alpha, 1]) = [2\alpha, 1]$. For $\alpha = 0.75$, $2 - 2\alpha = 0.5$, one has $\Phi^2(0) = 0.5$ and $\Phi^2(0.5) = 0.5$. ■

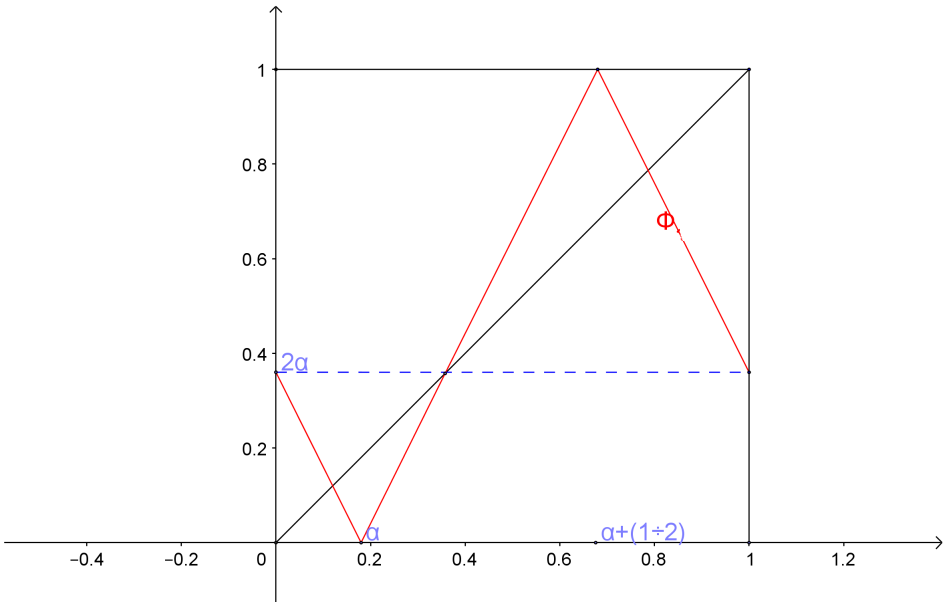

Figure 17. Graph of the Poincaré map Φ for $\alpha < \frac{1}{2}$.

5. Geometrical mug-shaped model: The general case

In previous sections, the simplest case of the geometrical mug-shaped model has been thoroughly studied. In this simplest case, *bursting* oscillations are mixing of *bursts* of U and W *spikes*. However, it is possible to model *bursting* oscillations which mix *bursts* of any number of *spikes*. In this section, an example of the extension of the simplest case model is given to demonstrate this possibility. In this example, oscillations mix *bursts* of 4 to 8 *spikes*.

The main idea to extend the simplest model is to split the interval of injection into several intervals, while leaving the interval of reinjection unchanged.

5.1. *Split interval of injection*

To explain the extended geometrical model using an example (Fig. 23), let $s = 1.4$ and the interval of injection be a union of four subintervals:

$I_s^r = [2.1, 2.4[\cup[2.4, 2.5[\cup[3.8, 4.1[\cup[5.5, 5.8[$.

When a trajectory on the cylinder reaches for $x = -1$ the subinterval $[1.4, 2.1[$, it cannot escape to the ribbon and must continue to turn around the cylinder, except when it reaches the first subinterval $[2.1, 2.4[$. The trajectory which continues on the cylinder can eventually escape through the window of the second subinterval $[2.4, 2.5[$ or the next one $[3.8, 4.1[$ or $[5.5, 5.8[$.

The interval of reinjection has the same definition as for the simplest model case:

$I_s^c = [-2.4, -1.4[$.

Keeping the same notation of Sec. 2, on each half-plane H_m, the parabolic trajectory is always parametrized by θ following Eq. (14).

$$\begin{cases} \tilde{X}_m(\theta) = \frac{M\theta}{T}(2-\theta), & \\ \tilde{Z}_m(\theta) = -\frac{3.8}{2T}\theta + z_m^r & \text{for} \quad z_m^r \in [2.1, 2.4[, \\ \tilde{Z}_m(\theta) = -\frac{4.8}{2T}\theta + z_m^r & \text{for} \quad z_m^r \in [2.4, 2.5[, \\ \tilde{Z}_m(\theta) = -\frac{5.8}{2T}\theta + z_m^r & \text{for} \quad z_m^r \in [3.8, 4.1[, \\ \tilde{Z}_m(\theta) = -\frac{7.8}{2T}\theta + z_m^r & \text{for} \quad z_m^r \in [5.5, 5.8[. \end{cases} \tag{52}$$

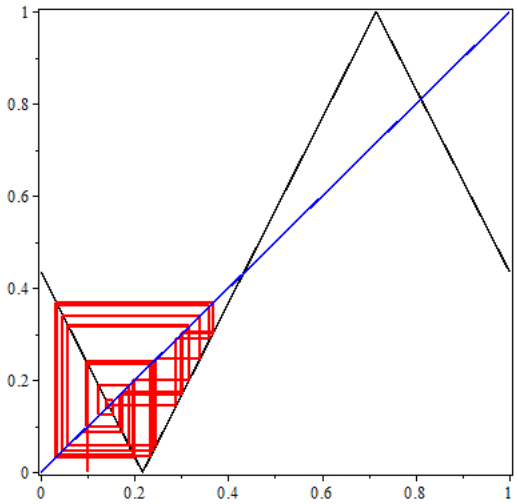

Figure 18. Graphical iterations for the map Φ when $\alpha < \frac{1}{2}$ and for initial condition $\zeta_0 = 0.1$

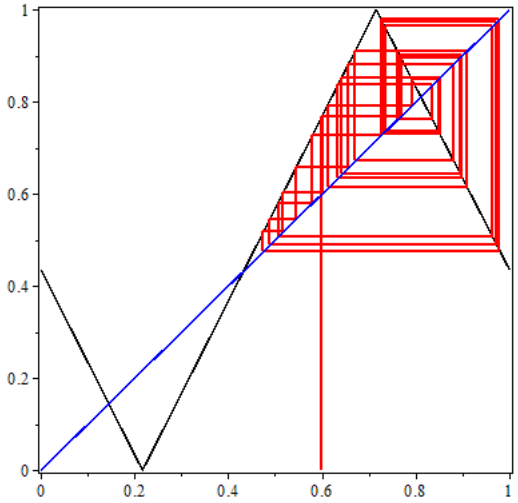

Figure 19. Graphical iterations for the map Φ when $\alpha < \frac{1}{2}$ and for initial condition $\zeta_0 = 0.6$

Therefore, the half-Poincaré map Ψ_2 is defined as

$$\begin{cases} \Psi_2(z) = z - (2s+1) & \text{for} \quad z_m^r \in [2.1, 2.4[, \\ \Psi_2(z) = z - (2s+2) & \text{for} \quad z_m^r \in [2.4, 2.5[, \\ \Psi_2(z) = z - (2s+3) & \text{for} \quad z_m^r \in [3.8, 4.1[, \\ \Psi_2(z) = z - (2s+5) & \text{for} \quad z_m^r \in [5.5, 5.8[. \end{cases} \tag{53}$$

Figure 23 displays a first periodic orbit with initial point $z = -2.1$.

This orbit intersects the border of the cylinder $x = \{-1\}$ for the following values of z: $-2.1 \to -1.1 \to -0.1 \to 0.9 \to 1.9 \to 2.9 \to 3.9$ and escapes from the cylinder to the ribbon from the subinterval $[3.8, 4.1[$ after 6 *spikes*.

After that, the orbit is back on the cylinder at the point $z = -1.9$ and intersects again the border of the cylinder $x = \{-1\}$ for the following values of z: $-1.9 \to -0.9 \to 0.1 \to 1.1 \to 2.1$ escaping to the ribbon after 4 *spikes* from the subinterval $[2.1, 2.4[$, and so on, being again on the cylinder for $z = -1.7 \to -0.7 \to 0.3 \to 1.3 \to 2.3$ escaping again from the subinterval $[2.1, 2.4[$, after 4 *spikes* to the ribbon and then on the cylinder for $z = -1.5 \to -0.5 \to 0.5 \to 1.5 \to 2.5 \to 3.5 \to 4.5 \to 5.5$ escaping

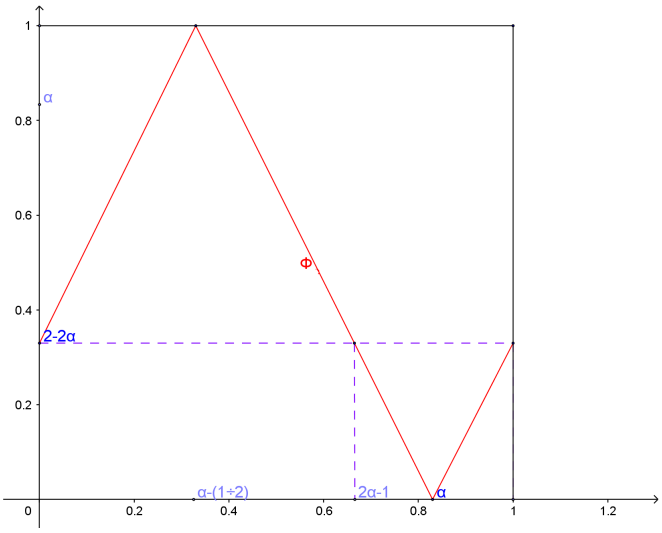

Figure 20. Graph of the Poincaré map Φ for $\alpha > \frac{1}{2}$.

again from the subinterval $[5.5, 5.8[$ after 7 *spikes*, being one more time on the cylinder for $z = -2.3 \to -1.3 \to -0.3 \to 0.7 \to 1.7 \to 2.7 \to 3.7 \to 4.7 \to 5.7$ escaping one more time from the subinterval $[5.5, 5.8[$ after 8 *spikes* and returning to the initial value $z = -2.1$. For this periodic orbit, the *bursts* are successively containing 6, 4, 4, 7 and 8 *spikes*.

5.2. *Coexisting periodic solutions*

More interestingly in this example, two periodic solutions with different patterns can coexist. The second periodic orbit starts with the initial point $z = -1.6$, and has the following pattern:

$-1.6 \to -0.6 \to 0.4 \to 1.4 \to 2.4$ exit $[2.4, 2.5[$ after 4 *spikes*,
$-2.4 \to -1.4 \to -0.4 \to 0.6 \to 1.6 \to 2.6 \to 3.6 \to 4.6 \to 5.6$ exit $[5.5, 5.8[$ after 8 *spikes*,
$-2.2 \to -1.2 \to -0.2 \to 0.8 \to 1.8 \to 2.8 \to 3.8$ exit $[3.8, 4.1[$ after 6 *spikes*,
$-2 \to -1 \to 0 \to 1 \to 2 \to 3 \to 4$ exit $[3.8, 4.1[$ after 6 *spikes*,
$-1.8 \to -0.8 \to 0.2 \to 1.2 \to 2.2$ exit $[2.1, 2.4[$ after 4 *spikes* and back to the initial value $z = -1.6$.

The *bursts* are composed of 4, 8, 6, 6, 4 *spikes*.

The above two examples of coexisting periodic *bursting* orbits, exhibiting different patterns, show the extraordinary versatility of this generalized model.

Depending on the shape of the injection interval, more coexisting *bursting* orbits, either periodic of quasiperiodic, could coexist.

6. Conclusion

In this paper, a simplest bursting neuron model is introduced, based on the Hodgkin-Huxley and Hindmarsh-Rose models, with a geometric mug-shaped branched manifold, which can mix burst of n and $n+1$ spikes. The model can generate complex dynamic patterns, including periodic and quasiperiodic orbits. Rigorous analytic proofs of their existence are given, and their complex dynamics are discussed with clear graphical demonstrations. Furthermore, a more complex case of the model, which can generate chaotic bursting orbits with n and $n+1$ spikes, is established and discussed. The model is generalized to obtain mixing burst of any number of spikes. Finally, an example with bursts of 4 to 8 spikes is demonstrated. The advantage of the new model is its simplicity in form with complex dynamics, presenting most neuron burst patterns for complete analysis.

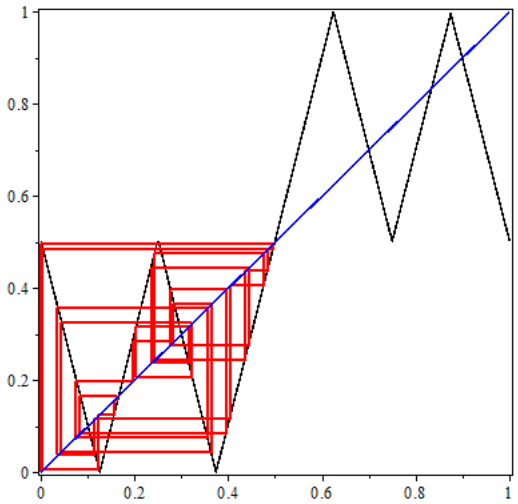

Figure 21. Graphical iterations for the map Φ^2 when $\alpha = 0.75$ and for initial condition $\zeta_0 = 0.001$

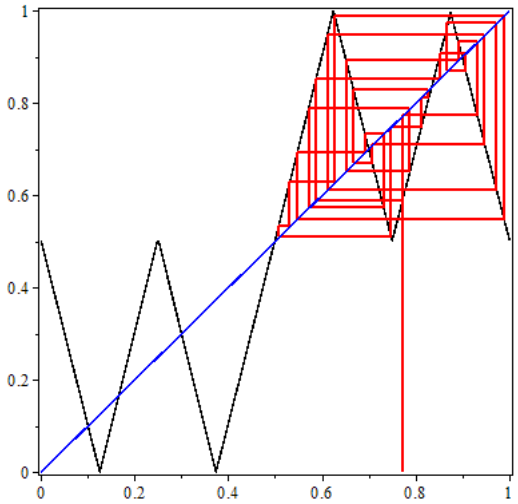

Figure 22. Graphical iterations for the map Φ^2 when $\alpha = 0.75$ and for initial condition $\zeta_0 = 0.772$

References

Abdelouahab, M.-S., Lozi, R., Chen, G. [2019] "Complex canard explosion in a fractional-order FitzHugh-Nagumo model", *International Journal of Bifurcation and Chaos*, **29**, No. 8, 1950111 (22 pages).

Corson, N. [2009] *Dynamique d'un modèle neuronal, synchronisation et complexité, thèse de Doctorat d'Etat*, (Université du Havre).

Devaney R. L. [2003] *An Introduction to Chaotic Dynamical Systems*, Addison-Wesley Publishing Company, Inc.

Hindmarsh, J. L., Rose, R. M. [1982] "A model of the nerve impulse using two first-order differential equations,"*Nature.* **296**, pp. 162–164.

Hindmarsh, J .L., Rose, R. M. [1984] "A model of neuronal bursting using three coupled first order differential equations,"*Proc. R. Soc. London B.* **221**, pp. 87–102.

Hodgkin, A. L. & Huxley, A. F. [1952] "A quantitative description of membrane current and its application to conduction and excitation in nerve,"*J. Physiol.* **117**, pp. 500–544.

Shilnikov, A. L. & Rulkov, N. F. [2003] "Origin of chaos in a two-dimensional map modelling spiking-bursting neural activity,"*International Journal of Bifurcation and Chaos.* **13**, pp. 3325–3340.

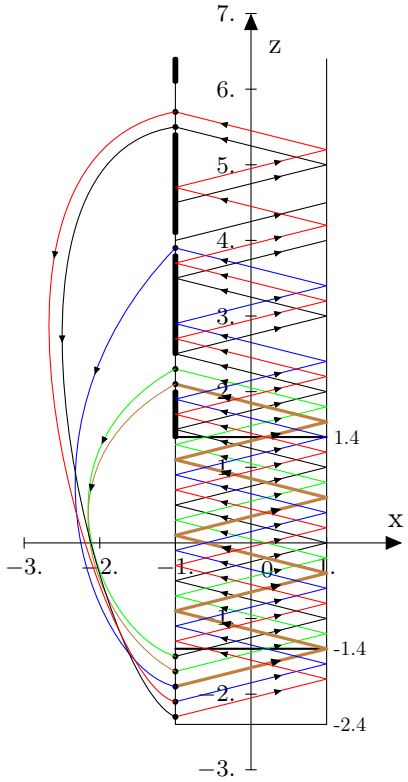

Figure 23. Periodic orbit of the generalized mug-shaped model for $s = 1.4$, initial value $z = -2.1$.

.

Shilnikov, A. L. & Kolomiets, M. [2008] "Methods of the qualitative theory for the Hindmarsh-Model: A case study.A Tutorial,"*International Journal of Bifurcation and Chaos.* **18**, pp. 2141–2168.

Izhikevich, E. M. [2007] *Dynamical Systems in Neuroscience: The Geometry of Excitability and Bursting*, The MIT Press Cambridge, Massachusetts, London, England.

Stiles, J. & Jernigan, T. J. [2010] "The Basics of Brain Development,"*Neuropsychol. Rev.* **4**, pp. 327–348.

Weyl, H. [1916] "Uber die Gleichverteilung von Zahlen mod. Eins, *Mathematische Annalen*, **77**, no. 3, pp. 313–352.